

Mechanical forces orchestrate the metabolism of the developing oilseed rape embryo

Hardy Rolletschek¹, Aleksandra Muszynska^{1,2}, Jörg Schwender³, Volodymyr Radchuk¹, Björn Heinemann⁴ D, Alexander Hilo¹ D, Iaroslav Plutenko¹ D, Peter Keil¹ D, Stefan Ortleb¹ D, Steffen Wagner¹ D, Laura Kalms¹ D, André Gündel^{1,5} D, Hai Shi³ D, Jörg Fuchs¹ D, Jedrzej Jakub Szymanski^{1,6,7} D, Hans-Peter Braun⁴ D and Ljudmilla Borisjuk¹

¹Leibniz-Institute of Plant Genetics and Crop Plant Research (IPK), Corrensstrasse 3, Seeland, OT Gatersleben, 06466, Germany; ²Amatera Biosciences, 4 rue Pierre Fontaine, Evry, 91000, France; ³Biology Department, Brookhaven National Laboratory, Upton, NY 11973, USA; ⁴Institut für Pflanzengenetik, Universität Hannover, Herrenhäuser Strasse, Hannover, 30419, Germany; 5Department of Ecology, Environment and Plant Sciences, University of Stockholm, Stockholm, 10691, Sweden; 6Institute of Bio- and Geosciences, IBG-4: Bioinformatics, Forschungszentrum Jülich, Jülich, D-52428, Germany; ⁷Cluster of Excellence on Plant Sciences (CEPLAS), Heinrich-Heine-Universität Düsseldorf, Düsseldorf, 40225, Germany

Authors for correspondence: Hardy Rolletschek Email: rollet@ipk-gatersleben.de

Liudmilla Borisiuk Email: borysyuk@ipk-gatersleben.de

Received: 10 March 2024 Accepted: 18 June 2024

New Phytologist (2024) 244: 1328-1344 doi: 10.1111/nph.19990

Key words: Brassica napus, computer graphic reconstruction, embryogenesis, maturation, mechanical stress, morphogenesis, MRI, transcription factors.

Summary

- The initial free expansion of the embryo within a seed is at some point inhibited by its contact with the testa, resulting in its formation of folds and borders. Although less obvious, mechanical forces appear to trigger and accelerate seed maturation. However, the mechanistic basis for this effect remains unclear.
- Manipulation of the mechanical constraints affecting either the in vivo or in vitro growth of oilseed rape embryos was combined with analytical approaches, including magnetic resonance imaging and computer graphic reconstruction, immunolabelling, flow cytometry, transcriptomic, proteomic, lipidomic and metabolomic profiling.
- Our data implied that, in vivo, the imposition of mechanical restraints impeded the expansion of testa and endosperm, resulting in the embryo's deformation. An acceleration in embryonic development was implied by the cessation of cell proliferation and the stimulation of lipid and protein storage, characteristic of embryo maturation. The underlying molecular signature included elements of cell cycle control, reactive oxygen species metabolism and transcriptional reprogramming, along with allosteric control of glycolytic flux. Constricting the space allowed for the expansion of *in vitro* grown embryos induced a similar response.
- The conclusion is that the imposition of mechanical constraints over the growth of the developing oilseed rape embryo provides an important trigger for its maturation.

Introduction

Mechanical forces, such as those generated by touch and pressure, are known to induce the production of a specific set of cellular products (Murthy et al., 2017). Elucidating the biology of mechanosensing has recently been awarded with the Nobel Prize in Physiology or Medicine (Ledford & Callaway, 2021). Tissue differentiation and morphogenesis are influenced by mechanical forces and mechanosensing (Radlanski & Renz, 2006), as is the determination of the size of the mammalian embryo (Chan et al., 2019). Plants are thought to exploit similar means to sense mechanical forces (Radin et al., 2021) - dozens of mechanosensitive channel proteins have been described, responsible for a range of responses (Hamilton et al., 2015; Basu & Haswell, 2017; Farmer et al., 2020), and affecting a multitude of physiological functions and developmental processes (Hamant & Moulia, 2016; Landrein & Ingram, 2019; Coen & Cosgrove, 2023), including the process of seed development (Creff et al., 2015, 2023; Fourquin et al., 2016; Rolletschek et al., 2021b).

In nonseed vascular plants, such as the ferns, the embryo develops within a soft gametophyte, providing an environment lacking any constraint to its expansion; however, in angiosperms, the embryo developed in a spatially confined environment. The expanding embryo abuts the embryo sac, forcing it to bend and fold (Borisjuk et al., 2013). Assuming that the young embryo has some flexibility (as growing pollen tubes; Vogler et al., 2013), it can react to a physical obstruction by adjusting its direction of growth. The importance of mechanosensing-induced proteins to this deformation is not known, nor is the means by which embryonic cells adjust their metabolism in response to mechanical stress. The key point is that embryonic cells are not free to follow an intrinsic differentiation programme, but rather are forced to adapt to the space within which their growth has placed them; not only does this affect the embryo's final shape and size, but also it may also have an impact on its progress towards

maturation. In oilseed rape (*Brassica napus*), maturation is dominated by the accumulation of lipids and proteins (Borisjuk *et al.*, 2013). The process is generally held to be tightly controlled, largely by the action of transcriptional master regulators, microRNAs, abscisic acid (ABA) and sugars (Willmann *et al.*, 2011; Belmonte *et al.*, 2013; Baud *et al.*, 2016; Leprince *et al.*, 2017; O'Neill *et al.*, 2019).

Recent data acquired from developing oilseed rape embryos imply that it responds to physical restraint by accelerating its storage metabolism (Rolletschek et al., 2021b). However, the molecular and biochemical basis of this response remained unknown. The aim here was to reveal the mechanisms underlying this response. A contrast was drawn between embryos grown under spatially restricted and nonrestricted conditions, employing magnetic resonance imaging (MRI) to noninvasively track the process of embryogenesis. The experimental data were used to build an in silico-based model of seed growth, which in turn allowed for the visualization of the embryo's response to the imposition of mechanical constraint. In parallel, transcriptomic, proteomic, lipidomic and metabolomic data, as well as a flow cytometrybased analysis of embryonic cell number, were used to characterize morphogenesis. The analysis identified the involvement of multiple transcriptional regulators, hormonal action and metabolic switches in the embryonic response, leading to a conclusion that mechanical stimuli indeed represent a key input to the embryo maturation process.

Materials and Methods

Plant material and growth conditions

Plants of oilseed rape (*Brassica napus* L. cultivar Reston) were grown in a glasshouse under a temperature regime of $22 \pm 2^{\circ}$ C, a 16 h photoperiod (250 mmol quanta m⁻² s⁻¹) and 60% relative humidity. Seed set was accomplished using manual pollination.

Experimental approaches for space restriction *in vivo* and *in vitro*

Both an in vitro and an in vivo approach was used to impede the embryo's growth, as outlined by Rolletschek et al. (2021b). For the former, intact embryos at the cotyledon stage of development (c. 23 d after flowering (DAF)) were aseptically removed from the silique and transferred to a liquid culture for 1 d under 50 μmol quanta m⁻² s⁻¹ at 23°C. The culture medium contained a source of organic nitrogen, sucrose, mineral salts and 15% polyethylene glycol, following Schwender et al. (2015). The embryos were then transferred into spherical chambers of variable diameter (Supporting Information Fig. S1), where they were allowed to grow in a nutrient-rich medium for a further 15 d, after which they were weighed and freeze-dried. The high temperature resin (type flhtam01 and flhtam02) chambers were formed using a Formlabs-2 3D printer, and were perforated to allow for the free flow of medium and gas. The ready-to-use models are provided in the Methods \$1 (STL-formatted files for standard CAD software). For the *in vivo* experiments, a 2 cm length of silicone tube (internal diameter 3 mm) was partially wound *c*. a 10 DAF silique, thereby reducing the space available for the expansion of the seed in the restricted part of the silique (Fig. S2a). Siliques, harvested at distinct time intervals, were either subjected to MRI, or were dissected to recover intact seeds and embryos; the set of samples collected comprised 'space-restricted' samples (those seeds experiencing constrained growth), 'internal control' samples (iCRT: nonrestricted seeds sampled from the unbound segment of a bound silique) and 'external control' siliques (eCRT: nonrestricted seeds sampled from an unbound silique).

MRI

Magnetic resonance imaging data were generated using a Bruker Avance IIITM HD 400 MHz NMR spectrometer (Bruker BioSpin GmbH & Co. KG, Ettlingen, Germany) equipped with a 1000 mT m⁻¹ gradient system and resonators with inner diameters of 5 and 10 mm. A spin echo sequence tailored to visualise water and lipid simultaneously was used to display the threedimensional morphology and volumetric analysis of live seeds, following Munz et al. (2017). Global frequency-selective RF pulses ("calculated" shape with bandwidth 1500 Hz) facilitated the separate excitation of water and lipid. An interleaved acquisition scheme was conducted as described elsewhere (Munz et al., 2016). For the 3D MRI of live seeds within a silique, an isotropic resolution of 70 µm was applied by applying the following parameters: repetition time (TR) of 400 ms; echo time (TE) 6 ms; number of averages (NA) 4; field of view (FOV) 11 \times 7.5 \times 7.5 mm³; matrix size 157 \times 107 \times 107. Some measurements were conducted with the same sequence parameters but a larger FOV (30 \times 14.5 \times 14.5 mm³, matrix size 375 \times 181 \times 181) and NA = 1. Image reconstruction was performed using MATLAB software (MathWorks, https://www. mathworks.com/).

Analysing seed development using computer graphic reconstruction

A virtual reconstruction of the oilseed rape embryo's morphogenesis was used to compare and display the morphometric changes occurring inside a seed subjected to space restriction with those occurring in a seed not experiencing any space restriction. The generation of digital volumetric twins for the seeds was performed using the open-source 3D editor BLENDER v.2.81 (Blender Development Team; BLENDER, v.2.81, www.blender.org). The constituent parts of the seed (testa, embryo, radicle, inner and outer cotyledon) were identified using software AMIRA3D (v.2022.1, Thermo Fisher Scientific, Schwerte, Germany) then imported into Blender. Unit settings of the 3D editor were set to maintain the resolution of the original data during the reconstruction process. The imported objects served as a reference for recreating a simplified topology, taking care to preserving the shapes, volumes and ratios of the major organs. Having prepared the meshes for key stages and ensuring that they shared a similar structure in terms of vertex, edges, and face count, the transition between the various stages was animated using the Shape Keys feature. The scripting module was used to assess the volume of objects (seed components) and its spatiotemporal variations.

Profiling the metabolome, proteome and lipidome

All procedures used for tissue extraction and the parameters chosen for analysis are detailed in Methods S2. In short, metabolite profiling was applied to chloroform/methanol/water extracted embryo samples using liquid chromatography coupled to high-resolution mass spectrometry (MS). Proteome analysis of seed material was done using label-free quantitative shotgun MS. For lipid profiling, embryo material was extracted using chloroform/methanol/water mixtures, followed by gas chromatography-MS (for quantitative analysis of triacylglycerols and fatty acid profiling) and liquid chromatography-MS (for profiling of phospholipids and neutral lipids).

Mature seed analysis

Seeds were harvested at maturity and stored at 4°C. The lipid content in c. 40 mg seed tissue was measured in at least ten biological replicates using an mq60 time domain NMR device (Bruker GmbH, Rheinstetten, Germany) following Borisjuk et al. (2013). Seed dimensions were determined using a MARVIN seed analyser (GTA Sensorik GmbH, Neubrandenburg, Germany). Germination was tested using a standard protocol (Rolletschek et al., 2020).

RNA extraction, reverse transcription and qPCR

Total RNA was isolated using Trizol reagent (Thermo Fisher Scientific), treated with DNase (Qiagen) and purified using an RNeasy kit (Qiagen). Reverse transcription into single-stranded cDNA was achieved using a QuantiTect Reverse Transcription kit (Qiagen). Quantitative polymerase chain reactions were performed with a QuantStudio 6 Flex Real-Time PCR system (Applied Biosystems Deutschland GmbH, Darmstadt, Germany) using a PowerUp SYBR Green Master Mix (Applied Biosystems). Relative mRNA abundances were determined using the $\Delta\Delta$ CT method and normalized to that of the oilseed rape gene encoding ubiquitin-conjugating enzyme 21, following Chen *et al.* (2010). The primer sequences are given in Table S1. Each experiment included either three or four biological replicates (each comprising ten embryos), along with three technical repetitions per biological replicate.

RNA sequencing

RNA was extracted as described above (three biological replicates each comprising ten embryos), processed using the TruSeq RNA Kit (Illumina, San Diego, CA, USA) following the manufacturer's instructions. The resulting libraries were sequenced using an Illumina HiSeqTM 2500 high-throughput flow cell. Adapter trimming was performed using CUTADAPT software

(Martin, 2011). Read mapping was performed on the *Brassica napus* Ensembl v.47 genome and the same version of the annotation file (Chalhoub *et al.*, 2014) using the software package HISAT2 (Kim *et al.*, 2015). Data normalization, filtering and differential expression were performed using the R package EDGER (Robinson *et al.*, 2010). Differential transcription thresholds were set at *P* adjusted value < 0.05. The *P*-values were adjusted for multiple testing using the Benjamini–Hochberg false discovery rate correction formula. Functional enrichment analysis to determine enrichment of Gene Ontology (GO) terms was done using the Database for Annotation, Visualization and Integrated Discovery (DAVID) web tool (Sherman *et al.*, 2022). Since *B. napus* is not recognized as an organism by the database, gene IDs of *Arabidopsis* gene homologs were submitted for analysis.

Immunolabelling

Immunostaining was done as described by Borisjuk *et al.* (2013). Primary polyclonal antibodies raised in rabbit against oleosin1 or oleosin2 were purchased from PhytoAB Inc. (San Jose, CA, USA). Fluorescence intensities of oleosin 1 and 2 were recorded with a Zeiss LSM780 confocal laser scanning microscope (Carl Zeiss GmbH, Jena, Germany) using a $20\times$ N.A. 0.8 objective with optimal resolution setting and pinhole 32 μ m. Probes were scanned with a 488 nm laser line and fluorescence recorded between 490 and 597 nm using a lambda-detector. After spectral unmixing average pixel intensity of Alexa 488 positive signals were measured using the Zeiss Zen black software edition 3.2.

Flow cytometry

Embryos were dissected from seeds grown *in vivo* for 25, 30 or 35 DAF either in the presence or absence of space restriction, and from those grown *in vitro* collected after 15 d of culture in either space-restricted (Ø 3 mm or 5 mm spheres) or under nonrestricted conditions; each sample comprised ten embryos. The number of cells within a given embryo was estimated using flow cytometry: nuclei were isolated in an isolation buffer (Galbraith *et al.*, 1983) supplemented with 50 μg ml⁻¹ propidium iodide and 50 μg ml⁻¹ DNase-free RNase, as described by Doležel *et al.* (2007). The cell counting device was a CyFlow Space flow cytometer (Sysmex-Partec, Münster, Germany), set up to run the 'Partec True Volumetric Absolute Counting' function. Data acquisition and analysis was performed using FLOMAX Software v.2.82 (Quantum Analysis GmbH, Münster-Gievenbeck, Germany).

Statistics

Microsoft Excel 2019 and Matlab software (v.R2019b; http://www.mathworks.com) were used to perform statistical calculations, applying an alpha value of 0.05; relevant tests and replicate numbers are shown in the appropriate Figure legends. To run a principal component analysis (PCA), the data were processed using Matlab v.9.9.0.1592791 R2020b, using the function "pca" and default settings (singular value decomposition algorithm, data centring).

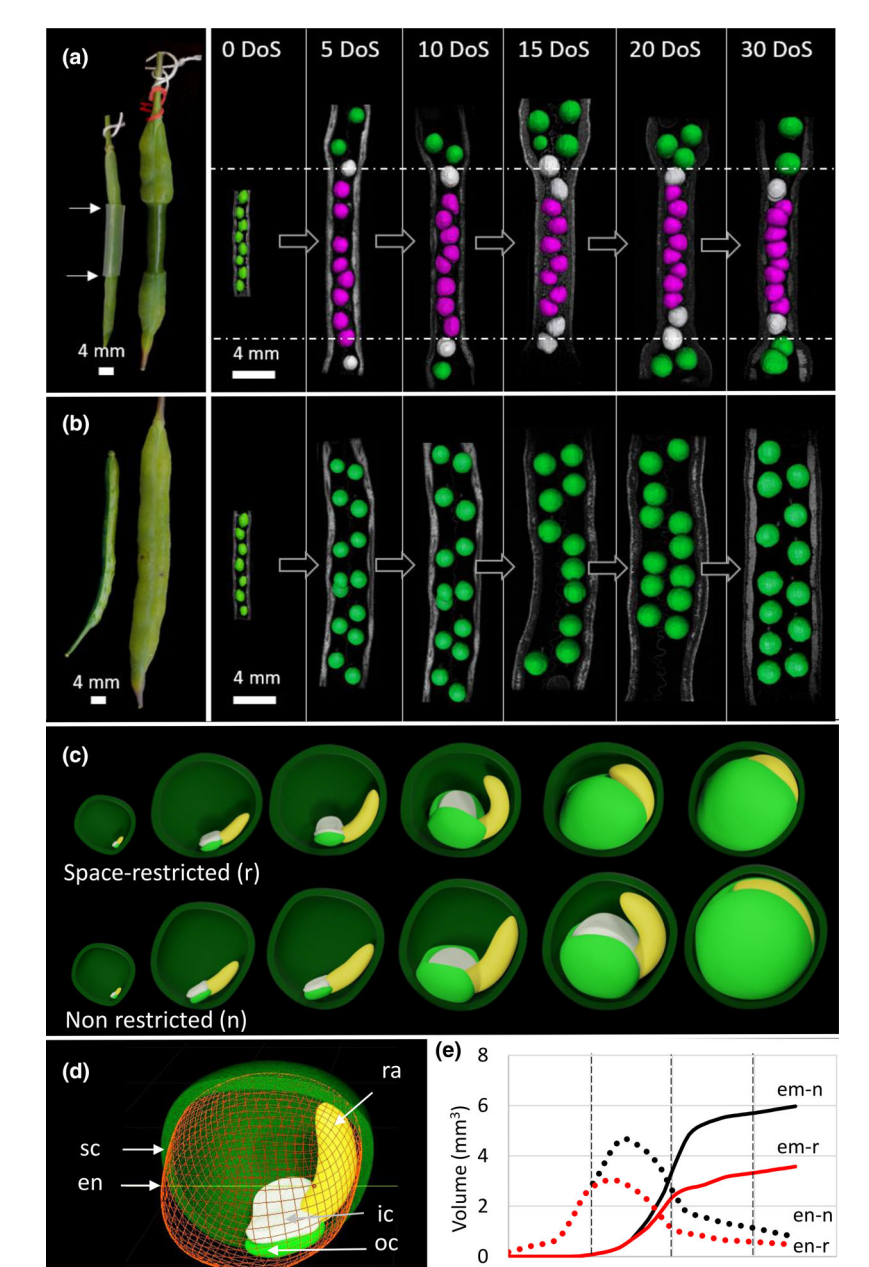


Fig. 1 The effect of space restriction on embryogenesis in Brassica napus. (a, b) On the left, photographic images showing a silique bound with tubing (indicated by white arrows) to reduce the space available for seed expansion (a) and a neighbouring silique without mechanical constriction (external control) (b); siliques at the start and end of the experiment. On the right, MRI-based noninvasive visualization of seeds growing in the space-restricted region of a silique (in red), in the bordering region (in grey) and of those growing outside the constriction (in green, internal control) assayed after 0, 5, 10, 15, 20 and 30 d following the imposition of stress (DoS). Individual siliques were imaged and harvested at the indicated time points. (c) Computer graphics reconstruction displaying the dynamics of seed growth under restrictive (upper panel) and nonrestrictive (lower panel) conditions showing the progression of embryo bending and folding (for colour scheme see (d)); the full developmental sequence is shown in Supporting Information Video S1. (d) 3D model showing individual seed components. (e) Volumes of the endosperm (dotted line) and embryo (solid line) during seed development under restrictive (in red) and under nonrestrictive (in black) growing conditions. em, embryo; en, endosperm; ic, inner cotyledon; oc, outer cotyledon; ra, radicle; sc, testa.

Results

Mechanical stress affects the course of embryogenesis

Winding tubing around an intact 10 DAF silique successfully hindered its expansion, consequently reducing the space available for the developing seed to expand into (Fig. 1a,b). A virtual model of the growth response of the embryo, based on the MRI-based tracking of the embryogenesis process, illustrated the effect of mechanical restriction over the seed's expansion (Fig. 1c–e; Video S1). During the first 10 d following the imposition of stress (10 DoS equivalent to 10–20 DAF) there was no significant treatment effect, since up to this point, there was no difference in the either the size of the seed formed or the

developmental stage reached by the embryo (Fig. S2); in both control and space-restricted treatment, embryos first initiated the radicle and cotyledons (becoming heart-shaped), then developed into a torpedo-shaped structure as a result of the elongation of the embryo and the formation of the cotyledons. As development proceeded, the siliques thickened, which in the case of the bound siliques, resulted in a gradual reduction in the space available for the seed's expansion. The effect of this restriction was a marked slowing of the seed's enlargement; in the unbound (control) siliques, seed growth continued unabated, so that by 15 DoS, a size notably greater than that of seed experiencing the mechanical stress had been reached (Fig. S2b). Computer graphic reconstruction revealed that the onset of deformation occurred earlier and progressed faster in embryos forming in the treated siliques than

10

20

30

DoS

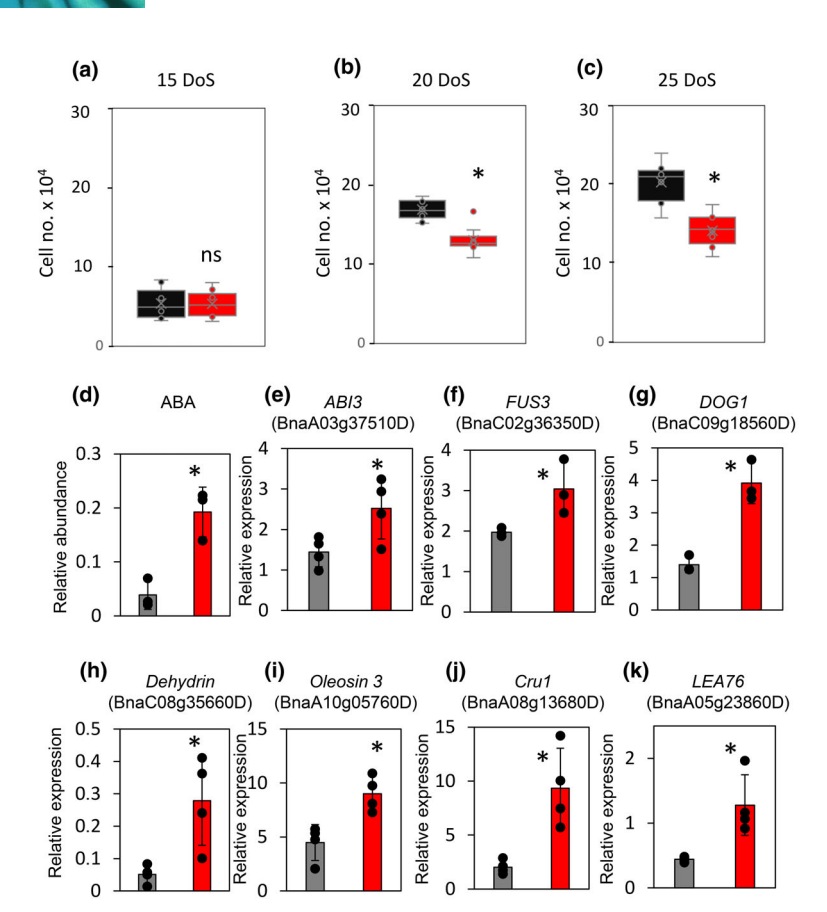


Fig. 2 Cell proliferation, gene expression and ABA content in embryos of *Brassica napus* grown *in vivo* under space restriction. (a–c) The cell number of embryos measured using flow cytometry 15, 20 and 25 d after the imposition of mechanical stress (DoS) (in red) and in those growing under stress-free conditions (in black). Box-whisker plots show the mean, median, quartiles and SD (n=10). (d) Relative levels of ABA in the embryo (black, nonstressed control; red, stress treatment) measured using LC–MS after 15 DoS. (e–k) Transcript abundance of selected genes after 15 DoS, as estimated using quantitative PCR. All data given in relative units and presented in the form mean \pm SD; dots indicate individual samples. Transcript abundances normalized to that of *ubc21*. Asterisks indicate statistical significance (P < 0.05; n = 4; Kruskal–Wallis test); ns, not statistically significant.

in the nonstressed ones (Fig. 1c; a full sequence is given in Video S1). At the time point when the embryos developing in the bound siliques had fully occupied the space available to them, the cotyledons in the seeds developing in the nonbound siliques were still expanding. Data implied that the endosperm responds to a restriction in space much earlier than does the embryo (Fig. 1e), and that the expansion of the endosperm ceased earlier in space-restricted seeds. The overall conclusion was that reducing the space available for the embryo to expand induces its premature deformation.

Space restriction reduces cell proliferation in the embryo

The cell number of embryos dissected from 15, 20 and 25 DoS seeds was established using flow cytometry. The 15–25 DoS time span extends from the end of the rapid cell proliferation phase until the transition into cell expansion. While a similar cell number obtained in the treated and control embryos at 15 DoS (Fig. 2a), by 20 DoS, the number in the former had doubled, while that in the latter had tripled (Fig. 2b). The difference was maintained in 25 DoS embryos (Fig. 2c). The indication is that that restricting the growth of the embryo impairs cell proliferation.

Space-restricted embryos experience a slowing of cell division but an acceleration in maturation

The transcriptome of stressed and nonstressed embryos sampled at 10 and 15 DoS was acquired using RNA-Seq (Table S2). In

the 10 DoS embryos, the transcripts of only three genes (encoding a 12S seed storage protein, a metallothionein 2A and an S12/ S23 ribosomal protein) were differentially abundant between the treated vs control embryos. However, in the 15 DoS embryos, this number had increased to 76 (49 less abundant and 27 more abundant in the treated embryos) (Tables 1, S2). GO enrichment analysis indicated 'Cellular Response to Hypoxia' as being significantly downregulated and 'Sulphate assimilation' as upregulated under mechanical restriction (Table S2f). The largest group of downregulated genes comprised 15 encoding stress-related proteins (three hypoxia-related genes and several chaperones). The next largest group (12 genes) encoded proteins involved in cell proliferation, including eight diverse histones. As revealed by quantitative reverse transcription polymerase chain reaction analysis, the genes encoding cyclin-dependent protein kinases 3;2 and B2;1 as well as cyclins B1;2 and B1;3, the core proteins of cell cycle (Boruc et al., 2010), were also downregulated (Fig. S3). The gene subtilase 3.13 (encoding a serine protease involved in cell cycle control, D'Erfurth et al., 2012) was among the most strongly downregulated genes. Four genes encoding components of photosynthesis were also downregulated. The largest group of genes more abundantly transcribed in the stressed embryos included sulphate transporter 3;4 (Ding et al., 2015), ATP sulfurylase 1, sulphite reductase, both homeologs of disulphide isomerase, nitrile specifier protein 5 and β -glucosidase 28, all of which encode products involved in glucosinolate synthesis (Yatusevich et al., 2010). The implication is that mechanically stressed embryos experienced an increased sulphur demand, generally associated

https://nph.onlinelibrary.wiley.com/doi/10.1111/nph.19990 by Forschungszentrum Jülich GmbH Research Center, Wiley Online Library on [15/11/2024]. See the Terms

Table 1 Differential expression of selected genes in embryos of Brassica napus sampled after 15 d of stress treatment in vivo compared with controls

Gene ID oilseed rape	Gene ID of Arabidopsis homolog	Gene description	e description Fold change in expression (log ₂)	
Genes upregulated	under mechanical restriction			
BnaA07g37260D	AT5G07470	Peptidemethionine sulfoxide reductase 3	7.09	0.006
BnaA10g01440D	AT1G02850	β-glucosidase 11	6.38	0.048
BnaA10g24180D	AT5G06760	Late embryogenesis abundant protein, LEA4-5	4.37	0.073
BnaA07g37340D	AT1G21310	Extensin 3	4.23	0.073
BnaA03g02060D	AT5G07470	Peptidemethionine sulfoxide reductase 3	4.04	0.002
BnaC02g38780D	AT5G48850	Sulphur deficiency-induced 1	3.86	0.056
BnaA05g04030D	AT2G44460	β-glucosidase 28	3.78	0.000
BnaC05g28620D	AT1G32450	Nitrate transporter 1.5	3.37	0.080
BnaC06g33240D	AT1G72180	C-terminally encoded peptide receptor 2	2.68	0.094
BnaA04g21240D	AT2G37040	Phenylalanine ammonia-lyase	1.86	0.024
BnaC01g04250D	AT4G34131	UDP-glucosyl transferase 73B3	1.80	0.009
BnaA06g25040D	AT5G67470	Formin homolog 6	1.78	0.073
BnaCnng62800D	AT3G22890	ATP sulfurylase 1	1.76	0.002
BnaA03g36860D	AT3G22890	ATP sulfurylase 1	1.74	0.052
BnaC06g14990D	AT3G53990	Universal stress protein 18, USP17	1.74	0.004
BnaA04g21230D	AT2G37040	Phenylalanine ammonia-lyase	1.61	0.055
BnaC01g02340D	AT4G36360	β-galactosidase 3	1.43	0.053
BnaC02g18350D	AT1G68560	α-xylosidase 1	1.28	0.006
BnaA10g05760D	AT5G51210	Oleosin3	1.27	0.100
BnaA01g28310D	AT3G15990	Sulphate transporter 3;4	1.24	0.047
U	ed under mechanical restricti			
BnaA07g30180D	AT1G72430	SAUR-like auxin-responsive protein family	-1.28	0.053
BnaC04g13850D	AT2G30620	Histone H1	-1.30	0.032
BnaA10g04420D	AT2G30620	Histone H1	-1.24	0.011
BnaAnng01620D	AT5G06150	Cyclin B1;2	-1.50	0.069
BnaA03g09170D	AT3G45980	Histone superfamily protein	-1.62	0.004
BnaC06g24340D	AT1G72430	SAUR-like auxin-responsive protein 78	-1.72	0.080
BnaA05g33830D	AT3G01480	Cyclophilin 38	-1.87	0.024
BnaC03g11480D	AT3G45980	Histone H2B	-1.90	0.011
BnaA03g50170D	AT4G30440	UDP-D-glucuronate 4-epimerase 1	-1.95	0.024
BnaC08g40890D	AT1G12820	Auxin signalling F-box 3	-2.32	0.024
BnaA09g53380D	AT5G65360	Histone H3.1	-2.85	0.006
BnaA08g18750D	AT1G27770	ACA1, chloroplast envelope Ca ²⁺ -ATPase	-2.92	0.054
BnaA01g11480D	AT4G21650	Subtilase family protein SBT3.13	-7.06	0.012
BnaC09g36140D	AT5G22920	Ubiquitin E3 ligase RZFP34/CHYR1	-7.83	0.004

Colour indicates upregulation (in red) and downregulation (in blue).

with the synthesis of both storage proteins and glucosinolates. Oilseed rape seed proteins are generally abundant in sulphurcontaining amino acids (Hannoufa et al., 2014), and the accumulation of glucosinolates in the embryo is a recognized landmark of seed maturation (Meier et al., 2019). A further three genes encoding proteins involved in amino acid metabolism (phenylalanine ammonia-lyase, proline-tRNA ligase and glutamine amidotransferase) were also upregulated. Among the most strongly upregulated genes were five encoding peptidemethionine sulfoxide reductase—the enzyme responsible for the repair of oxidatively damaged proteins (Châtelain et al., 2013) — along with universal stress protein 17 and UDP-glucosyl transferase 73B3, the products of which mirror the redox status of cells experiencing stress (Jung et al., 2015; Rehman et al., 2018).

Seed maturation, signalled by the accumulation of storage compounds, is mediated by both hormones (principally abscisic acid (ABA)) and transcriptional master regulators (Baud et al., 2016). A LC-MS-based analysis revealed that a higher level of ABA was present in the stressed than in the nonstressed embryos at 15 DoS (Fig. 2d). Consistent with this was a higher abundance of transcript, as detected by quantitative PCR analysis, of ABI 3 (ABA insensitive 3, encoding a regulator of a number of genes related to seed storage, see Mönke et al., 2012), DOG1 (delay of germination 1, which encodes a positive regulator of ABA signalling, see Dekkers et al., 2016) and FUSCA 3 (FUS3, an activator of oil accumulation, see Yang et al., 2022) transcription factors (Fig. 2e-g). A similar upregulation of dehydrin, oleosin 3, cruciferin 1 and late abundant protein 76 was noted in the stressed embryos (Fig. 2h-k). However, the treatment had no effect on the transcription of any of LEAFY COTYLEDON 1-LIKE, LEAFY COTYLEDON 2, DOG1-LIKE 4 or WRINKLED 1 (Fig. S3), nor on that of other known mechanosensing-related genes (Table S1e).

In essence, the data indicate that imposing a mechanical constraint on the embryo had the effect of repressing cell cycle activity, while promoting storage product synthesis/accumulation, ROS defence mechanisms and ABA-related signalling.

Alterations in the space-restricted embryo metabolome imply an accelerated glycolytic flux and the provision of lipid precursors

Targeted and untargeted metabolite profiling of embryos grown *in vivo* and sampled at 5, 10, 15, 20, 25 and 30 DoS identified 152 metabolic intermediates (Table S3a). A principal component analysis was unable to differentiate between the three treatments: space-restricted, iCRT and eCRT (Fig. S4), but close inspection of the data indicated that the treatment affected the glycolytic pathway (Fig. 3). The level of fructose-1,6-diphosphate and its two cleavage products dihydroxyacetone-phosphate and glyceraldehyde-3-phosphate were all remarkably higher in the stressed embryos at 15 DoS and/or at 20 DoS. The level of the triacylglycerol (TAG) synthesis precursor glycerol-3-phosphate (G3P) was elevated in 15 DoS embryos by as much as ninefold, although the genes encoding G3P dehydrogenase were not noticeably upregulated (Table S2d). Both of the more downstream glycolysis products 3-PGA (3-phosphoglycerate) and PEP

(phosphoenolpyruvate) were significantly less abundant in both 10 and 15 DoS stressed embryos than in the nonstressed ones; a reduced level of these two compounds has been identified as an indicator of elevated glycolytic pathway flux (Schwender *et al.*, 2015).

Mechanical restriction promotes the onset of storage lipid deposition

Three-dimensional MRI-based seed and lipid models showed that, after 15 DoS, in vivo grown seeds experiencing space restriction accumulated more total lipid than those growing without any restriction (Fig. S5). However, this difference was transient in nature (not seen at 35 DoS). Lipid profiling of 15 DoS embryos identified the presence of 170 lipid species (64 TAGs, 16 diacylglycerols (DAGs), and 90 phospholipids) (Table S4). The TAG content was 17–38% higher in the stressed than in the nonstressed embryos (Fig. S6a), notably because of an enhanced presence of oleic (C18:1) and eicosenoic (C20:1) acids, accompanied by a reduced representation of higher saturated fatty acids (Fig. S6b). There was also a noticeable compositional shift for some individual TAGs and DAGs (Fig. S6d,e). Phospholipids accounted for c. 1% of the embryo's biomass, but there was no clear treatment effect on the content of phosphatidylcholine, phosphatidylethanolamine, phosphatidylglycerol, phosphatidic acid or phosphatidylinositol (Fig. S6c). The conclusion was that space restriction promoted the onset of storage lipid deposition, but had no effect on other lipid classes.

Space restriction promotes central metabolic pathways, including storage product synthesis

The use of quantitative shotgun mass spectrometry to monitor the seeds' proteomic response to the space restriction treatment revealed that the content of 61 (out of 1189) proteins differed between treated and control seeds sampled at 10 DoS, as were 25 (out of 1173) in seeds sampled at 15 DoS (Fig. 4; Table S5). There was a substantial degree of overlap between the time points: most prominently, the treatment stimulated protein storage deposition, with seven RmlC-like cupins, seed storage albumin 4 and cruciferin 1 all showing an up to fivefold increase in content in response to the stress. In addition, a heightened abundance was noted for enzymes involved in amino acid synthesis (aspartate aminotransferase, pyridoxal phosphate-dependent transferases superfamily protein), in lipid synthesis/storage (embryo-specific 3-ketoacyl-CoA synthase, 3-ketoacyl-(acylcarrier-protein) reductase, enoyl-(acyl-carrier-protein) reductase, lipid droplet-associated protein 3, biotin carboxylase, acyl-(acylcarrier-protein) desaturase), in sugar metabolism (sucrose synthase, glucose-6-phosphate 1-dehydrogenase), in reactive oxygen species (ROS) metabolism (catalase, peroxidase superfamily protein) and in glycolysis (fructokinase, plastidial pyruvate α subunit and β subunit 1 – the latter two providing precursors for fatty acid synthesis). The stress suppressed by fourfold the accumulation of the embryo-specific, plasma membrane-associated TRAF-like family protein, a protein class related to central

Jülich GmbH Research Center, Wiley Online Library on [15/11/2024]. See the Terms

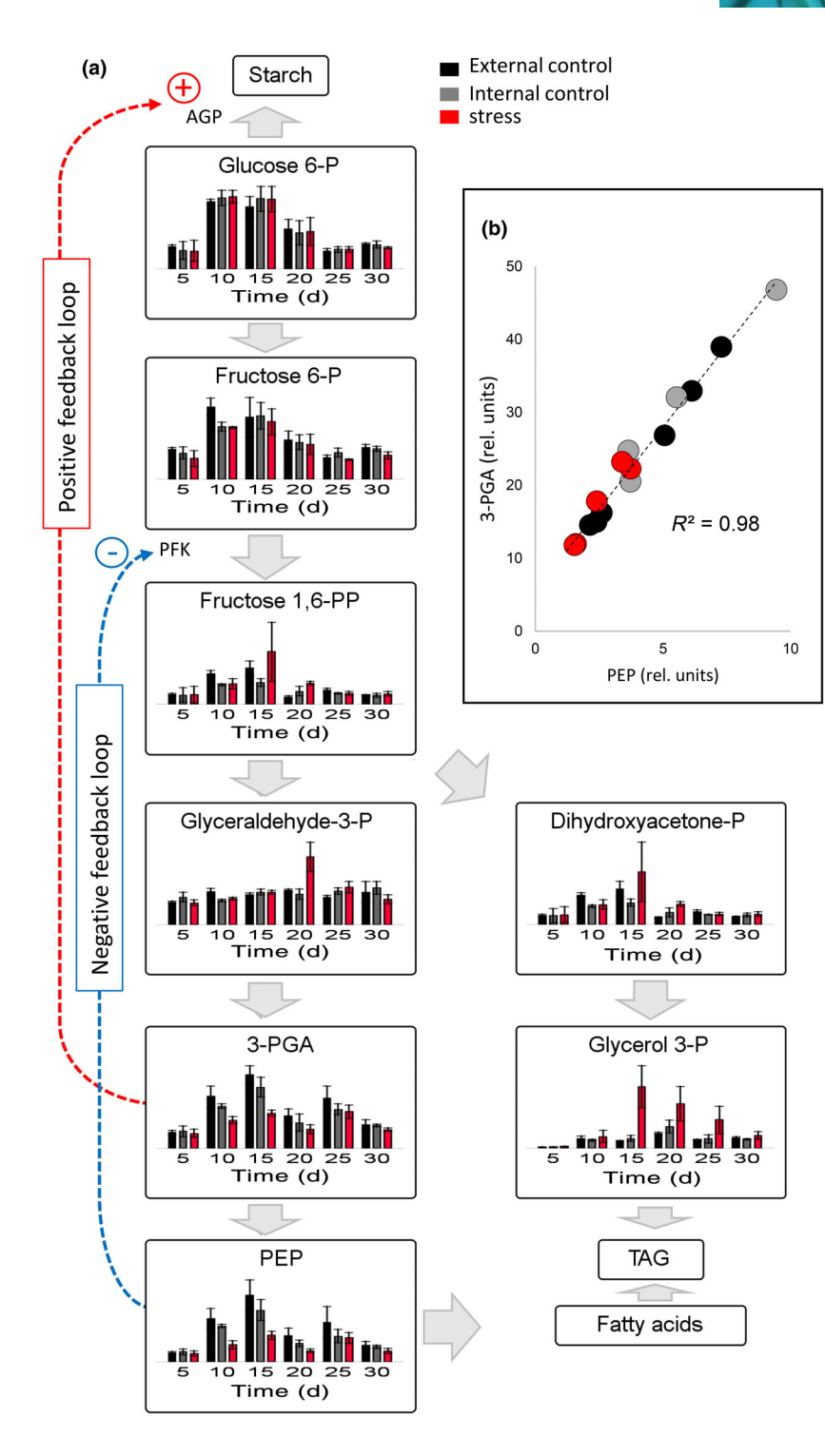
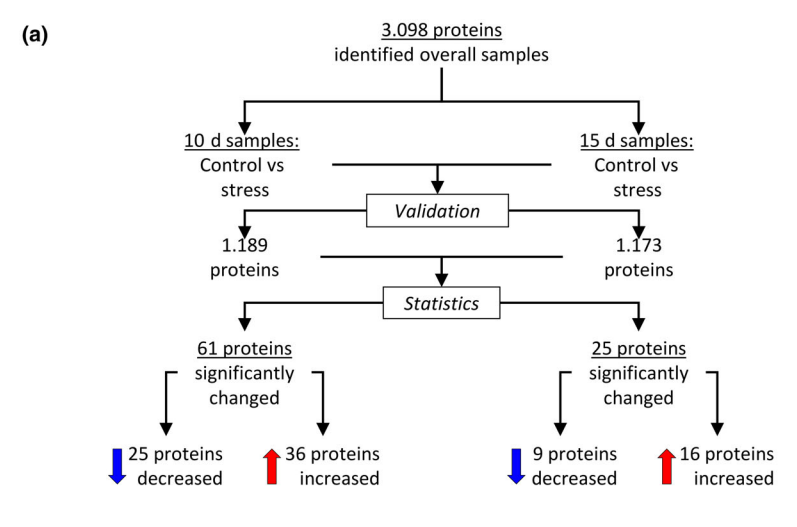


Fig. 3 The metabolome of embryos of *Brassica napus* grown *in vivo* under space restriction. (a) The relative abundance of metabolites produced within the glycolytic pathway, as measured by LC–MS. Embryos were isolated either following stress imposed by the mechanical constriction of the silique (stress), from a nonbound portion of the same silique (internal control) or from a neighbouring unbound silique (external control). Data given in the form mean ± SE; full statistical details are given in Supporting Information Table S3(c). (b) The abundance of the intermediates 3-phosphoglycerate (3-PGA) and phosphoenolpyruvate (PEP) were highly inter-correlated. AGP, ADP-glucose pyrophosphorylase; PFK, phosphofructokinase; TAG, triacylglycerols.

ABA-dependent signalling networks and the stress response (Qi et al., 2021). A number of the differentially accumulated proteins are known to be expressed also in either the testa or the endosperm (Table S5): examples are the downregulated proteins pectin methylesterase inhibitor, arabinogalactan protein 8 and beta-galactosidase 4, which are components of cell wall metabolism. It is possible that their differential abundance is related to the premature cessation of growth of testa and or endosperm induced by the imposition of mechanical stress (Fig. 1).

Mechanical restriction reduces the size but not the viability of the seed

Seeds grown to maturity under space-restricted conditions were smaller in size and somewhat irregularly shaped compared to those grown without the imposition of stress; they also featured a slightly lower (*c.* 10%) overall lipid content (Fig. S7). However, neither their rate nor speed of germination was compromised (Fig. S8).



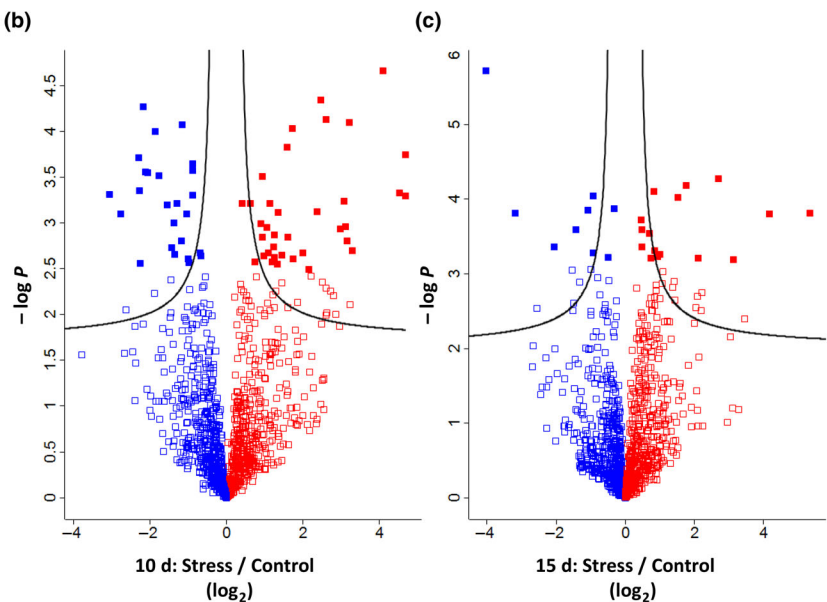


Fig. 4 Shifts in the seed proteome of Brassica napus after the imposition of space restriction in vivo. Quantitative shotgun mass spectrometry used to analyse the proteome of three biological replicates, each comprising c. 25 frozen seeds. (a) Workflow used to process the data. Only proteins identified in at least two replicates within a sample type were maintained. Volcano plots show the statistical significance ($-\log P$ value, t-test, false discovery rate (FDR): 0.05) and magnitude of proteins responding by a fold change in abundance following exposure to a stress period of (b) 10 d, (c) 15 d. Proteins identified as experiencing a significant fold change in abundance shown as filled squares. Red, more abundant in the stress samples, blue, less abundant in the stress samples. A full list of the proteins assayed is given in Supporting Information Table \$5.

The effect of space restriction on the growth of embryos cultured *in vitro*

To characterize the response of the seed to the imposition of space restriction independent of the influence of the maternal plant, excised embryos, isolated at the cotyledon stage, were cultured in purpose-built spherical chambers of various volumes (Fig. S1). The respective 3D-printed models are also provided in the Methods S1 (ready-to-use or for further customization using standard CAD programs). As described by Rolletschek *et al.* (2021b), the space constraint provoked a marked response, both with respect to the embryo's ability to increase its biomass and its ability to synthesize major storage products: the smaller the growing space, the smaller was the embryo and the greater was its lipid and protein content. In the following, we investigated these effects in more detail.

Folding of the embryos *in vitro* only occurred when their expansion was impeded by the chamber wall, that is under restricting chamber volumes (3.5 mm or below; Fig. 5a). MRI-based lipid mapping revealed that the most prominent region for deposition was in the upper hypocotyl (especially visible in

embryos raised in 3.5 mm chambers, Fig. 5b) and in the lower cotyledon tissues. Immunolabelling targeting Oleosin 1 and 2 (known to be markers of lipid deposition and maturation, Borisjuk *et al.*, 2013), revealed a higher accumulation of these proteins in mechanically restricted embryos vs those grown nonrestricted (Fig. 5c–f). When fluorescence intensity (green channel) was quantified, data revealed sixfold higher signals for Oleosin 1 (mean \pm SD: 25.6 \pm 3.5 vs 4.3 \pm 0.7) and fourfold higher signals for Oleosin 2 (13.2 \pm 2.5 vs 3.4 \pm 0.2) under mechanically restricted growth. This is in line with earlier observations that mechanically restricted embryos accumulated lipids both earlier and in greater amount than embryos whose growth was not impeded (Rolletschek *et al.*, 2021b).

The transcriptomic and cell proliferation responses of *in vitro* grown mechanically constrained embryos resembles those observed in *in vivo* grown materials

RNA sequencing of *in vitro* grown (3.5 mm chambers) embryos revealed that the abundance of 316 transcripts responded to the

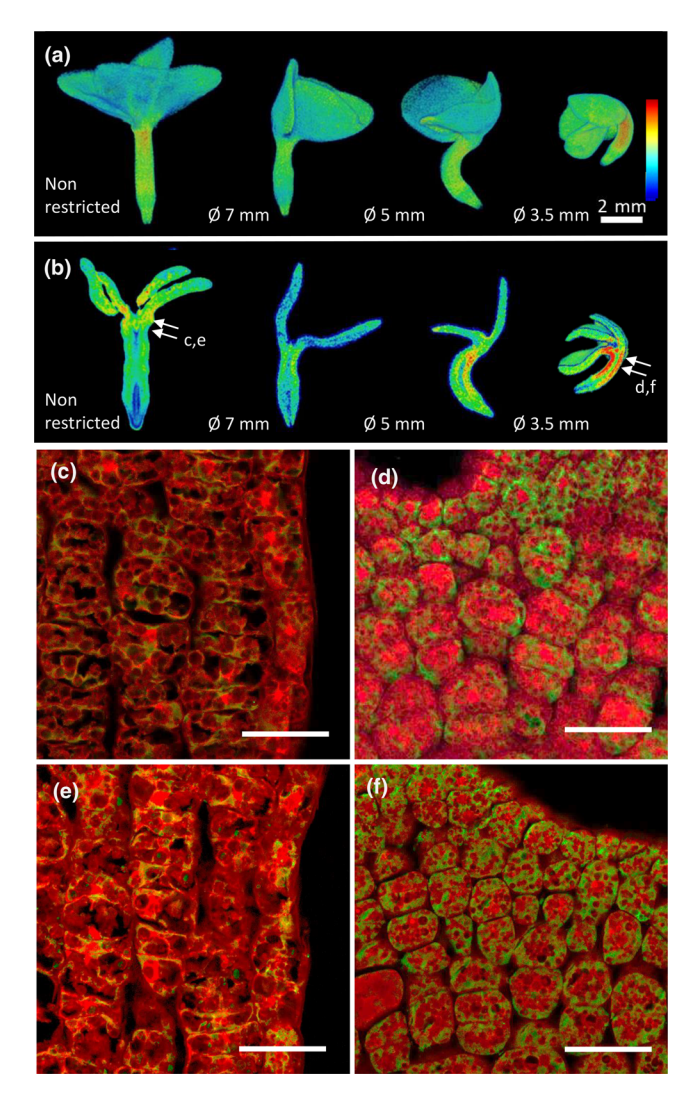
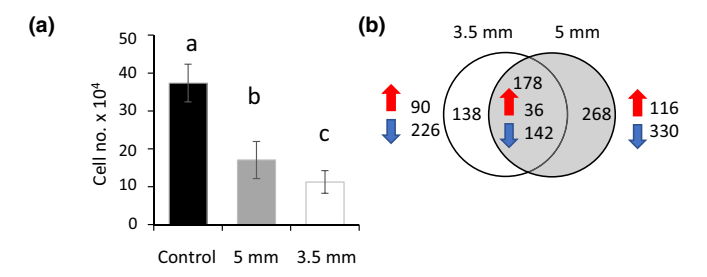


Fig. 5 The effect of space restriction on the growth and maturation of *Brassica napus* embryos cultured *in vitro*. (a) The distribution of lipids in embryos grown under varying space restriction conditions or under nonrestricted conditions; lipid concentrations, measured by MRI, are colour-coded (red = high, blue = low). (b) 2D lipid maps of virtual cross sections of the embryos shown in (a); arrows indicate regions used for immunolabelling using (c, d) oleosin 1, (e, f) oleosin 2. (c, e) nonrestricted embryos, (d, f) mechanically restricted embryos. Data obtained by CLSM; green, Alexa 488 conjugated with secondary antibody, red, autofluorescence; Bars: (c–f) 50 μm.

stress (90 positively, 226 negatively), while for embryos grown in 5 mm chambers, the number was 446 (116 positively, 330 negatively) (Fig. 6; Table S6). The two sets of differentially expressed genes have 178 genes in common (36 genes up vs 142 genes down), which is highly significant (hypergeometric P-value = 1E-144).

GO enrichment analysis revealed that photosynthesis was the major category which was statistically significantly downregulated under mechanical restriction (Table S6f). The downregulation of the gene encoding the GRAS family transcription factor SCARECROW-LIKE 28 (controlling the mitotic cell cycle and division plane orientation) together with that of two genes encoding patellin, SEC14 cytosolic factor (required for cell plate



Category		3.5-mm wells		5-mm wells	
	up	down	up	down	
Transcription factors	5	2	10	10	
Cell proliferation		24	-	24	
Photosynthesis, chloroplast and Calvin cycle		96	3	156	
Primary metabolism		4	-	12	
Secondary metabolism		4	4	7	
Transport	12	11	5	13	
Lipid metabolism	2	-	3	2	
Sugar metabolism	6	6	2	8	
Nitrogen metabolism	14	7	22	7	
Cell wall metabolism	-	7			
Stress-related	13	16	18	11	
Hormone-related	5	_	1	4	
Fe-related	4	6	3	14	
Others	21	30	38	46	
Unknown	7	12	8	16	

Fig. 6 The effect of space restriction on gene activity and cell number in embryos of Brassica napus cultured in vitro. (a) Cell numbers measured using flow cytometry, data given in the form mean \pm SD (n=10); different letters indicate a statistical significance between treatment groups (P < 0.05; Kruskal–Wallis test, followed by Bonferroni adjustment <math>post hoc test). (b) Venn diagram display showing the differentially transcribed genes (DEGs) unique to or shared between embryos grown in 3.5 or 5 mm spheres compared to nonrestricted controls. The number of DEGs shared between the treatments is shown in the intersecting region of the Venn diagram; the number of upregulated and downregulated DEGs is shown in, respectively, red and blue. A hypergeometric statistical test indicates that the number of DEGs shared between the two stress conditions (178) is 35 times higher than expected by random chance, giving a P-value of 1E-144. (c) Numbers of DEGs ordered by category. The full dataset is given in Supporting Information Table S6.

formation, embryo polarity and patterning, see Tejos et al., 2018) and two encoding expansin is indicative of a slowing of cell proliferation. The downregulation of both BARELY ANY MERISTEM 1 (BAM1), which encodes a CLAVATA1-related receptor kinase involved in the regulation of cell division and differentiation (DeYoung et al., 2006), and of somatic embryogenesis receptor kinase 1 (SERK1), which encodes a key control point for sporophytic development (Hecht et al., 2001), provides further support for this conclusion. Flow cytometric measurements clarified that the severity of the mechanical stress was inversely correlated with embryonic cell number (Fig. 6a).

An increased transcript abundance was induced for genes encoding oligopeptide transporters, glutamate dehydrogenase, glutathione S-transferase and LEA protein (three genes in the common set and 11 specific for embryos grown in the 5 mm chambers), suggestive of a promotion of storage compound metabolism. A developmental shut-off in starch synthesis was indicated by the observed fall in the transcript abundance of two genes encoding granule bound starch synthase. The upregulation of 13 genes encoding heat shock proteins (HSPs), especially in

14698137, 2024, 4, Downloaded

from https://nph.onlinelibrary.wiley.com/doi/10.1111/nph.19990 by Forschungs

entrum Jülich GmbH Research Center, Wiley Online Library on [15/11/2024]. See the Terms

Fig. 7 Metabolic pathway map highlights changes in metabolite abundances in embryos of *Brassica napus* grown *in vitro*. Embryos were isolated and cultured in spheres of varied internal diameter (as indicated in the legend). Metabolites were measured by LC–MS. Fold changes in abundance are colour coded: blue, lowered by space restriction; red, heightened by space restriction. Mean abundances (n = 5) used for calculation. The relevant metabolite data are provided in Supporting Information Table S3b.

the embryos grown in the 5 mm chambers, provided a further indication of premature embryo maturation (HSPs are a hall-mark of late seed maturation; see Leprince *et al.*, 2017). In line with the desiccation which is a feature of the maturing seed, two genes encoding proteins associated with water channel activity, namely *PIP3A* and *PIP3C*, were downregulated by both levels of stress, and further five PIP-encoding genes were downregulated in embryos grown in the 5 mm chambers. The abundance of *TPS1* transcript (encoding trehalose-6-phosphate (T6P) synthase, the key enzyme controlling levels of T6P) was also repressed in both the 3.5- and 5-mm treatments.

Multiple shifts in C/N metabolism are induced by space restriction

Metabolite profiling identified a set of 199 metabolic intermediates and hormones (Fig. 7; Table S3b). The space restriction induced the accumulation of energy-rich nucleoside triphosphates and cofactors, such as like pyridoxal-5-phosphate, flavin mononucleotide and nicotinamide adenine dinucleotide phosphate and organic acids (intermediates of the tricarboxylic acid cycle), short chain fatty acids, glutathione and its precursors and some phenolic acids (including benzoate as precursor for folate

biosynthesis (one-carbon-metabolism) with relevance to multiple cellular functions). In line with the outcome of the *in vivo* experiment, the level of the two glycolytic intermediates fructose-1,6-diphosphate and dihydroxyacetone-phosphate was promoted in the space-restricted embryos.

Mechanical restriction depleted almost all free amino acids (except asparagine) and polyamines (such as citrulline), trigonelline (pyridine nucleotide metabolism), lactate (fermentative metabolism) and ascorbate (main antioxidant). There was also a reduced presence of the sugar-signalling molecule T6P, likely related to transcriptional repression of TPS1. The stressed embryos harboured a significantly higher level of the ethylene precursor 1-aminocyclopropane-1-carboxylic acid, but there was no treatment effect on the content of the auxin indole-3-acetic acid. ABA was not detectable.

The overall impression was that the progressive mechanical restriction induced some specific shifts in C/N metabolism, most notably in nucleotide, cofactor and redox metabolism.

Discussion

Mechanical forces and constraints affect not just the embryo's shape but also its development and metabolism. The purpose of the present experiments was to shed light on the mechanistic basis of the embryo's response to mechanically imposed stress.

A mechanistic view on the timing and consequences of space restriction

In Brassicaceae species, the size of the seed is governed by the testa and the endosperm (Li et al., 2019). These two organs determine the space available for the embryo's growth. This space not only defines the embryo's metabolic environment (Rolletschek et al., 2021a), but also acts as a regulator of developmental progression, cell proliferation and maturation. Once fertilization has been achieved, a rapid proliferation, expansion and cellularization of the endosperm follows (Doll & Ingram, 2022). The cessation of the endosperm's expansion likely correlates with wall stiffening in the surrounding testa (Creff et al., 2023), thereby setting a size limit for the subsequent growth of the embryo. A tight tripartite interaction between the integuments, the endosperm and the embryo ensures the progress of development (Borisjuk et al., 2013; Figueiredo et al., 2016; Doll et al., 2020; Xu et al., 2023). When the seed's expansion was experimentally restricted in vivo, the endosperm's expansion ceased prematurely (Fig. 1e). The competition for space between the embryo and endosperm inhibited the embryo's elongation, prompting it to deform earlier than under control conditions (Fig. 1c; Video S1). A similar situation obtained in the in vitro experiment, which was designed to impose mechanical stress without any involvement of the testa/endosperm. Oilseed rape embryos allowed to grow freely in vitro do not bend, and even unfold rapidly when isolated from a developing seed and cultured in vitro (Rolletschek et al., 2021b). Thus, embryo shaping is a profoundly physical event, determined primarily by the space available for its expansion. In an earlier series of experiments, Borisjuk et al. (2013)

were able to show that the oilseed rape seed's architecture shapes its embryo's metabolism, while the imposition of a physical force can induce the deposition of storage products (Rolletschek et al., 2021b). Here, it has been shown that the application of a mechanical constraint, whether on in vivo or on in vitro grown embryos, shuts down cell proliferation and induces storage metabolism (Fig. 8); further, that the inevitable developmental onset of mechanical restriction, as imposed by the endosperm/testa, is an important trigger for the embryo's maturation programme. Seeds exposed to mechanical constraint grew to a smaller size, but their viability was unaffected (Figs 6, 7). The important implication is that the embryos' ability to coordinate mechanical, biochemical and physiological processes with the environment should be viewed as their ability to enhance plant fitness.

Mechanical restriction inhibits the embryo's cell cycle activity and induces the onset of seed maturation

In general, cell proliferation is a major determinant of size control. In mammals, tissue mechanics controls the shape and the size of the embryo, which is coupled to cell position and fate at the cellular scale (Piccolo, 2013; Chan et al., 2019). In plants too, feedback loops between cell division, mechanical stress and growth have been identified (Robinson, 2021). Here, it has been established that the developing oilseed rape embryo responded to physical restraint by reducing its final cell number (Figs 2, 6). A lower cell number is correlated with a reduced level of cell proliferation activity, primarily as a result of a slowing in cell cycle progression (Brioudes et al., 2010). Several potential means whereby mechanical restriction could negatively impact embryonic cell cycle activity have been identified by the present experiments, namely (1) the downregulation of genes encoding histones, subtilase 3.13 and others, essential for cell proliferation and its control, (2) a rise in the content of ABA, a hormone which bears down on embryonic cell division (Gutierrez, 2009); and (3) the downregulation of genes encoding the transcription factor SCARECROW-LIKE 28, the receptor kinases BAM1 and SERK1, subtilases, patellins and expansins, all of which have been linked to cell proliferation, embryo polarity and patterning. Last - but not least - the upregulation of FUS3, ABI3 and DOG1, which encode master regulators of maturation (Fig. 2), since their heightened activity likely would act to suppress embryonic cell cycle activity (Baud et al., 2016).

The transcription factors FUS3, ABI3, and DOG1 act together to mediate multiple aspects of the seed's maturation programme (Baud et al., 2016; Leprince et al., 2017). Their heightened activity in mechanically constrained embryos (Fig. 2) is clearly linked to the hastening of maturation induced by mechanical stress: as a result of their activity, oleosins, HSPs and LEA proteins are all accumulated (Baud et al., 2016; Dekkers et al., 2016). The latter proteins are important as molecular chaperones, enzyme protectants and antioxidants. ABI3/FUS3/DOG1 each act to upregulate genes encoding storage lipids and proteins (Dekkers et al., 2016; Yang et al., 2022). The accumulation of raffinose represents a further marker of the premature maturation of embryos experiencing space restriction

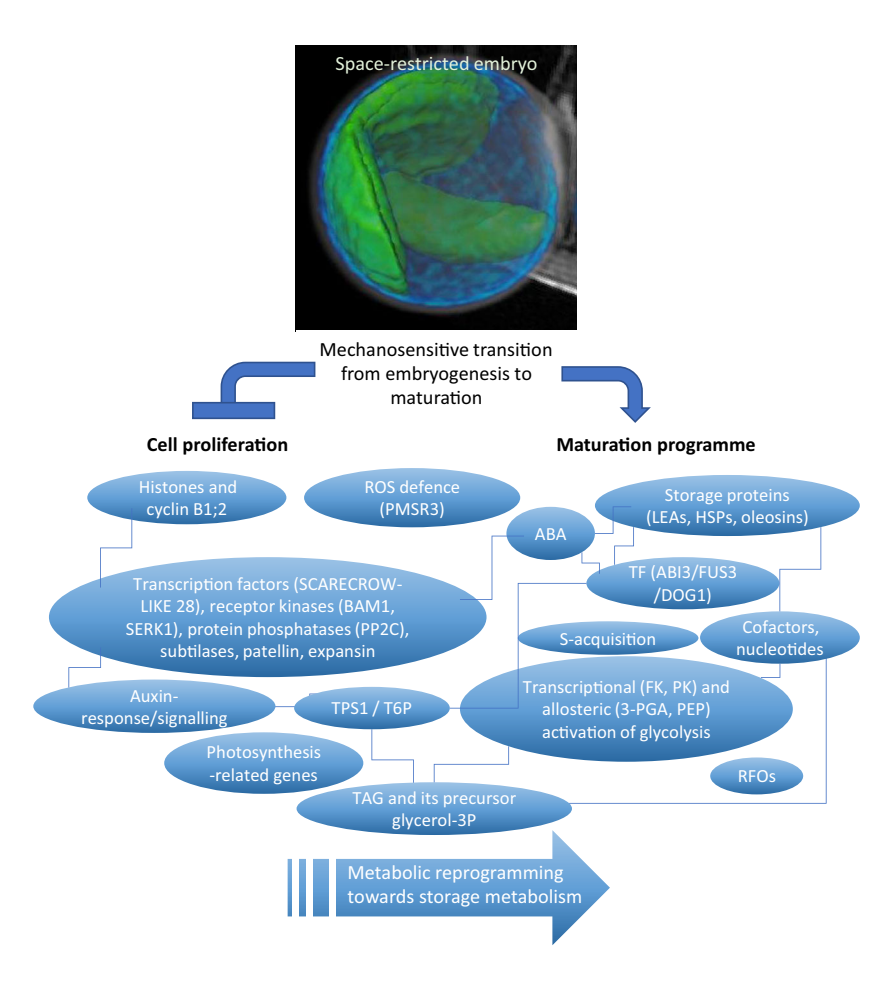


Fig. 8 A model for the mechanosensitive transition towards embryo maturation in oilseed rape (Brassica napus). The embryo develops in an environment spatially constrained by the integuments and the endosperm. The growing embryo adjusts its direction of growth within the seed, generating folds and borders. In parallel, the embryo responds to the physical restraint by shutting down cell proliferation and initiating its maturation programme. Potential key elements for the mechanosensitive transition detected in vivo and/or in vitro are shown. 3-PGA, 3-phosphoglycerate; ABA, abscisic acid; FK, fructokinase; PEP, phosphoenolpyruvate; PK, pyruvate kinase; PMSR3, peptide methionine sulfoxide reductase 3; RFOs, raffinose family oligosaccharides; T6P, trehalose-6phosphate; TAG, triacylglycerols; TF, transcription factors; TPS, trehalose-6P synthase. Blunt arrows (\perp) indicate inhibition while normal arrows (→) indicate stimulation.

(Rolletschek *et al.*, 2021b), as does the suppression of genes associated with photosynthesis.

Space restriction affects glycolysis and TAG synthesis by transcriptional and allosteric means

Maturation of the oilseed rape embryo requires the flow of carbon along the glycolytic pathway to be promoted, thereby feeding fatty acid and TAG synthesis (note that up to half of the rapeseed is composed of lipids). The present experiments revealed two distinct mechanisms whereby a mechanical stimulus is able to induce a higher glycolytic flux. First, it was apparent that mechanical stress induced a higher level of expression of proteins catalysing sugar cleavage, along with entry into and exit from the glycolytic pathway: the enzymes sucrose synthase, glucose-6phosphate dehydrogenase, fructokinase and plastidial pyruvate kinase. The greater abundance of glycolytic entry/exit proteins is important, as the relevant enzymatic steps have been shown in the oilseed rape embryo to be essentially irreversible (Schwender et al., 2015). This is in contrast to most of the other glycolytic steps, which are readily reversible (Schwender et al., 2015). Furthermore, an elevated abundance of several enzymes involved in lipid synthesis/storage was observed. The picture which emerges is that mechanical stimuli are translated into a transcriptionally mediated, pull-and-push strategy to enable the necessary

stimulation of metabolic flux from sugars into storage oils. Second, mechanical stress lowered the abundance of 3-PGA/PEP (Fig. 3), consistent with the bottom-up control of glycolytic flux (Schwender *et al.*, 2015): a lower level of 3-PGA leads to a reduction in the allosteric activation of AGPase, while a reduced level of PEP alleviates the allosteric repression of phosphofructokinase (PFK). The ratio of PEP and 3-PGA was fairly constant (Fig. 3), a pattern which has been previously noted in the developing oil-seed rape embryo (Schwender *et al.*, 2015). The suggestion is that an increased activity of pyruvate kinase lowers the level of both its substrate PEP and its upstream glycolytic intermediate 3-PGA, allowing their opposing effects on AGPase and PFK to occur simultaneously. The conclusion is that mechanical stimuli provide an allosteric means of controlling glycolytic flux.

In mammalian cells, mechanical forces have been reported to influence glycolytic flux in an additional, third way (Park et al., 2020). Specifically, where the extracellular matrix is soft, its interaction with the cytoskeleton activates the protein TRIM21, adding ubiquitin via E3 ubiquitin ligase to the glycolytic enzyme PFK. This tagging induces the degradation of PFK, leading to a reduced rate of glycolysis. By contrast, in the presence of a stiff matrix, stress fibres, composed of actin and myosin, act to trap TRIM21, thereby preventing the degradation of PFK. In our experiments, no significant effect with respect to the activity of genes encoding PFK, actin or distant homologs of TRIM21

could be detected in comparisons between the transcriptomes of mechanically stressed and nonstressed embryos. However, there was a transcriptional response in two cytoskeleton-related genes, namely *kinesin* 5 (Chen & Hancock, 2015) and *RZFP34/CHYR1*, which encodes a ubiquitin E3 ligase. Mechanical stress is known to strongly influence plant microtubule behaviour (Landrein & Hamant, 2013; Schneider *et al.*, 2022), but whether this affects glycolysis remains as yet unknown.

The level of the glycolysis intermediate G3P was elevated by some ninefold as a result of space restriction (Fig. 3). An excessive concentration of G3P in the oilseed rape seed is known to limit TAG synthesis (Vigeolas *et al.*, 2007). Possibly therefore, the increase in G3P level prompted by space restriction acts as an important inducer of TAG synthesis. Given the lack of a positive effect on the abundance of either *G3P dehydrogenase* transcript or its gene product, the potential shift in metabolic flux is likely related to an allosteric mode of control. Posttranslational modification of glycolytic enzymes, which are widespread, may also play a role (O'Leary & Plaxton, 2020).

Restricting the growth space of the embryo in vitro induced a marked accumulation of not just of numerous nucleotides/cofactors, but also of benzoate, a precursor of folate synthesis (Fig. 7). A plentiful supply of cofactors was shown by Hayden et al. (2011) to be strongly associated with an elevated flux into storage lipids and proteins. The reduction in the abundance of the signalling compound T6P observed in stressed embryos (Fig. 7), likely due to the downregulation of TPS1, could be relevant in this context. In the pea seed, a deficiency of T6P impairs starch synthesis, cotyledon growth and cell expansion (Meitzel et al., 2021), so the same may well also apply to the oilseed rape seed. While starch synthesis/degradation was not experimentally monitored in these experiments, it is known that the initiation of lipid storage in oilseed rape is accompanied by a decline in starch deposition (Borisjuk et al., 2013; Schwender et al., 2015). The hypothesis is therefore that starch synthesis is impaired upon the onset of space restriction, a process which is mediated by T6P.

How are mechanical stimuli perceived by the embryo?

Mechanical forces during the bending of the Arabidopsis thaliana root (adult plant) are known to induce the production of ROS (Monshausen et al., 2009). It has been shown here that embryo bending in oilseed rape was initiated earlier and occurred faster in seeds experiencing mechanical constraint (Fig. 1; Video S1). It is thus tempting to speculate that embryo bending is accompanied by a rise in oxidative stress, a notion corroborated by the marked changes in ROS metabolism induced by space restriction, both in in vivo raised and in in vitro cultured embryos. At the proteome level, mechanical stress resulted in a marked uplift in the level of a catalase and peroxidase superfamily protein, while at the transcriptional level there was a striking c. 130-fold upregulation of the gene encoding peptidemethionine sulfoxide reductase 3 (Table 1). Given that ROS oxidizes the sulphur-containing amino acid methionine to either methionine S-sulfoxide or methionine R-sulfoxide, the presence of peptidemethionine sulfoxide reductase 3 could help inhibit oxidative damage to cellular

proteins (Bechtold *et al.*, 2004; Hazra *et al.*, 2022). With respect to the metabolome, a strong depletion in both the major cellular antioxidant ascorbate and of trigonelline was observed (Fig. 7). The latter compound is thought to affect glutathione metabolism (Ashihara *et al.*, 2015). The overall conclusion is that the potential shifts induced by the imposition of mechanical stress in the seeds' oxidative homeostasis are consistent with those observed in other plant systems, in particular the bending of the *A. thaliana* root.

A few mechanosensing-related genes were expressed in the oil-seed rape embryo (Table S1e). What remains to be seen is the extent to which mechanosensing *sensu stricto* is involved in the embryonic growth response which occurs as a result of mechanical stress, and which mechanosensory proteins are employed. Addressing how physical forces induce cell signalling will require the elaboration of cell biology approaches.

Acknowledgements

This work was financially supported by the German Research Foundation (DFG) grant no. 397750294, the European Regional Development Fund (ERDF) and Investment Bank of Saxony-Anhalt (FKZ: ZS/2019/09/101444). JS and HS acknowledge funding by the US Department of Energy, Office of Science, Office of Basic Energy Sciences under contract number DE-SC0012704. We thank Dr Michele Salvi, Laura Goelckel and Heike Harms for experimental support. Open Access funding enabled and organized by Projekt DEAL.

Competing interests

None declared.

Author contributions

LB and HR designed the research, analysed the data and wrote the paper. AM performed sampling, immunolabelling and experimental work. HS and JS worked on lipid profiling, JS worked on metabolomics data and GO enrichment analysis, BH and H-PB worked on proteome profiling. VR, JS and JJS worked on RNA sequencing data. IP, SO, SW, LK and LB worked on MRI and computer graphics reconstruction. PK worked on statistics. AG worked on CAD-programming. JF performed flow cytometry. AH and HR worked on metabolite profiling. All authors have proofread and approved the manuscript.

ORCID

Ljudmilla Borisjuk https://orcid.org/0000-0001-6910-0841 Hans-Peter Braun https://orcid.org/0000-0002-4459-9727 Jörg Fuchs https://orcid.org/0000-0003-4171-5371 André Gündel https://orcid.org/0000-0003-1055-7577 Björn Heinemann https://orcid.org/0000-0002-3962-4174 Alexander Hilo https://orcid.org/0000-0002-7699-8060 Laura Kalms https://orcid.org/0009-0008-1977-0503 Peter Keil https://orcid.org/0000-0001-8398-4938

- Aleksandra Muszynska https://orcid.org/0000-0001-7589-7690
- Stefan Ortleb https://orcid.org/0000-0002-8655-0112

 Iaroslav Plutenko https://orcid.org/0000-0002-1064-3531

 Volodymyr Radchuk https://orcid.org/0000-0002-0472-6605
- Hardy Rolletschek https://orcid.org/0000-0002-8619-1391
 Jörg Schwender https://orcid.org/0000-0003-1350-4171
 Hai Shi https://orcid.org/0000-0002-7237-7777
 Jedrzej Jakub Szymanski https://orcid.org/0000-0003-1086-0920

Steffen Wagner https://orcid.org/0000-0001-5979-6013

Data availability

Primary proteome data are available at PRIDE (https://www.ebi.ac.uk/pride/archive/) under accession number PXD027763. Primary transcriptome data are available at the European Nucleotide Archive ENA (https://www.ebi.ac.uk/ena) under accession number PRJEB77373.

References

- Ashihara H, Ludwig IA, Katahira R, Yokota T, Fujimura T, Crozier A. 2015. Trigonelline and related nicotinic acid metabolites: occurrence, biosynthesis, taxonomic considerations, and their roles *in planta* and in human health. *Phytochemical Reviews* 14: 765–798.
- Basu D, Haswell ES. 2017. Plant mechanosensitive ion channels: an ocean of possibilities. Current Opinion in Plant Biology 40: 43–48.
- Baud S, Kelemen Z, Thevenin J, Boulard C, Blanchet S, To A, Payre M, Berger N, Effroy-Cuzzi D, Franco-Zorrilla JM et al. 2016. Deciphering the molecular mechanisms underpinning the transcriptional control of gene expression by master transcriptional regulators in Arabidopsis seed. Plant Physiology 171: 1099–1112.
- Bechtold U, Murphy DJ, Mullineaux PM. 2004. Arabidopsis peptide methionine sulfoxide reductase2 prevents cellular oxidative damage in long nights. Plant Cell 16: 908–919.
- Belmonte MF, Kirkbride RC, Stone SL, Pelletier JM, Bui AQ, Yeung EC, Hashimoto M, Fei J, Harada CM, Munoz MD et al. 2013. Comprehensive developmental profiles of gene activity in regions and subregions of the *Arabidopsis* seed. *Proceedings of the National Academy of Sciences, USA* 110: E435–E444.
- Borisjuk L, Neuberger T, Schwender J, Heinzel N, Sunderhaus S, Fuchs J, Hay JO, Tschiersch H, Braun HP, Denolf P *et al.* 2013. Seed architecture shapes embryo metabolism in oilseed rape. *Plant Cell* 25: 1625–1640.
- Boruc J, Van den Daele H, Hollunder J, Rombauts S, Mylle E, Hilson P, Inzé D, De Veylder L, Russinova E. 2010. Functional modules in the *Arabidopsis* core cell cycle binary protein-protein interaction network. *Plant Cell* 22: 1264–1280
- Brioudes F, Thierry AM, Chambrier P, Mollereau B, Bendahmane M. 2010. Translationally controlled tumor protein is a conserved mitotic growth integrator in animals and plants. *Proceedings of the National Academy of Sciences, USA* 107: 16384–16389.
- Chalhoub B, Denoeud F, Liu S, Parkin IA, Tang H, Wang X, Chiquet J, Belcram H, Tong C, Samans B et al. 2014. Plant genetics. Early allopolyploid evolution in the post-neolithic *Brassica napus* oilseed genome. *Science* 345: 950–953.
- Chan CJ, Costanzo M, Ruiz-Herrero T, Mönke G, Petrie RJ, Bergert M, Diz-Muñoz A, Mahadevan L, Hiiragi T. 2019. Hydraulic control of mammalian embryo size and cell fate. *Nature* 571: 112–116.
- Châtelain E, Satour P, Laugier E, Ly VB, Payet N, Rey P, Montrichard F. 2013. Evidence for participation of the methionine sulfoxide reductase repair system

- in plant seed longevity. *Proceedings of the National Academy of Sciences, USA* 110: 3633–3638.
- Chen X, Truksa M, Shah S, Weselake RJ. 2010. A survey of quantitative realtime polymerase chain reaction internal reference genes for expression studies in *Brassica napus. Analls of Biochemistry* 405: 138–140.
- Chen Y, Hancock WO. 2015. Kinesin-5 is a microtubule polymerase. Nature Communications 6: 8160.
- Coen E, Cosgrove DJ. 2023. The mechanics of plant morphogenesis. Science 379: 452
- Creff A, Ali O, Bied C, Bayle V, Ingram G, Landrein B. 2023. Evidence that endosperm turgor pressure both promotes and restricts seed growth and size. *Nature Communications* 14: 67.
- Creff A, Brocard L, Ingram G. 2015. A mechanically sensitive cell layer regulates the physical properties of the *Arabidopsis* seed coat. *Nature Communications* 6: 6382.
- Dekkers BJW, He H, Hanson J, Willems LAJ, Jamar DCL, Cueff G, Rajjou L, Hilhorst HWM, Bentsink L. 2016. The *Arabidopsis Delay of Germination 1* gene affects *Abscisic Acid Insensitive 5 (ABI5)* expression and genetically interacts with *ABI3* during *Arabidopsis* seed development. *The Plant Journal* 85: 451–465.
- D'Erfurth I, Le Signor C, Aubert G, Sanchez M, Vernoud V, Darchy B, Lherminier J, Bourion V, Bouteiller N, Bendahmane A et al. 2012. A role for an endosperm-localized subtilase in the control of seed size in legumes. New Phytologist 196: 738–751.
- DeYoung BJ, Bickle KL, Schrage KJ, Muskett P, Patel K, Clark SE. 2006. The CLAVATA1-related BAM1, BAM2 and BAM3 receptor kinase-like proteins are required for meristem function in *Arabidopsis. The Plant Journal* 45: 1–16.
- Ding S, Zhang B, Qin F. 2015. Arabidopsis RZFP34/CHYR1, a ubiquitin E3 ligase, regulates stomatal movement and drought tolerance via SnRK2.6mediated phosphorylation. *Plant Cell* 27: 3228–3244.
- Doležel J, Greilhuber J, Suda J. 2007. Estimation of nuclear DNA content in plants using flow cytometry. *Nature Protocols* 2: 2233–2244.
- Doll NM, Ingram GC. 2022. Embryo-endosperm interactions. Annual Review in Plant Biology 73: 293–321.
- Doll NM, Royek S, Fujita S, Okuda S, Chamot S, Stintzi A, Widiez T, Hothorn M, Schaller A, Geldner N et al. 2020. A two-way molecular dialogue between embryo and endosperm is required for seed development. Science 367: 431–435.
- Farmer EE, Gao YQ, Lenzoni G, Wolfender JL, Wu Q. 2020. Wound- and mechanostimulated electrical signals control hormone responses. *New Phytologist* 227: 1037–1050.
- Figueiredo DD, Batista RA, Roszak PJ, Hennig L, Köhler C. 2016. Auxin production in the endosperm drives seed coat development in *Arabidopsis. eLife* 5: e20542.
- Fourquin C, Beauzamy L, Chamot S, Creff A, Goodrich J, Boudaoud A, Ingram G. 2016. Mechanical stress mediated by both endosperm softening and embryo growth underlies endosperm elimination in *Arabidopsis* seeds. *Development* 143: 3300–3305.
- Galbraith DW, Harkins KR, Maddox JM, Ayres NM, Sharma DP, Firoozabady E. 1983. Rapid flow cytometric analysis of the cell cycle in intact plant tissues. *Science* 220: 1049–1051.
- Gutierrez C. 2009. The *Arabidopsis* cell division cycle. *Arabidopsis Book* 7: e0120. Hamant O, Moulia B. 2016. How do plants read their own shapes? *New Phytologist* 212: 333–337.
- Hamilton ES, Schlegel AM, Haswell ES. 2015. United in diversity: mechanosensitive ion channels in plants. Annual Review in Plant Biology 66: 113–137.
- Hannoufa A, Pillai BV, Chellamma S. 2014. Genetic enhancement of Brassica napus seed quality. Transgenic Research 23: 39–52.
- Hayden DM, Rolletschek H, Borisjuk L, Corwin J, Kliebenstein DJ, Grimberg A, Stymne S, Dehesh K. 2011. Cofactome analyses reveal enhanced flux of carbon into oil for potential biofuel production. *The Plant Journal* 67: 1018–1028.
- Hazra A, Varshney V, Verma P, Kamble NU, Ghosh S, Achary RK, Gautam S, Majee M. 2022. Methionine sulfoxide reductase B5 plays a key role in preserving seed vigor and longevity in rice (*Oryza sativa*). New Phytologist 236: 1042–1060.

s) on Wiley Online Library for rules of

- Hecht V, Vielle-Calzada JP, Hartog MV, Schmidt ED, Boutilier K, Grossniklaus U, de Vries SC. 2001. The *Arabidopsis* SOMATIC EMBRYOGENESIS RECEPTOR KINASE 1 gene is expressed in developing ovules and embryos and enhances embryogenic competence in culture. *Plant Physiology* 127: 803–816.
- Jung YJ, Melencion SM, Lee ES, Park JH, Alinapon CV, Oh HT, Yun DJ, Chi YH, Lee SY. 2015. Universal stress protein exhibits a redox-dependent chaperone function in *Arabidopsis* and enhances plant tolerance to heat shock and oxidative stress. *Frontiers in Plant Science* 6: 1141.
- Kim D, Langmead B, Salzberg SL. 2015. HISAT: a fast spliced aligner with low memory requirements. *Nature Methods* 12: 357–360.
- Landrein B, Hamant O. 2013. How mechanical stress controls microtubule behavior and morphogenesis in plants: history, experiments and revisited theories. *The Plant Journal* 75: 324–338.
- Landrein B, Ingram G. 2019. Connected through the force: mechanical signals in plant development. *Journal of Experimental Botany* 70: 3507–3519.
- Ledford H, Callaway E. 2021. Medicine nobel for duo who discovered biology of senses. *Nature* 598: 246.
- Leprince O, Pellizzaro A, Berriri S, Buitink J. 2017. Late seed maturation: drying without dying. *Journal of Experimental Botany* 68: 827–841.
- Li N, Xu R, Li Y. 2019. Molecular networks of seed size control in plants. *Annual Review of Plant Biology* 70: 435–463.
- Martin M. 2011. Cutadapt removes adapter sequences from high-throughput sequencing reads. EMBnet. Journal 17: 10–12.
- Meier K, Ehbrecht MD, Wittstock U. 2019. Glucosinolate content in dormant and germinating *Arabidopsis thaliana* seeds is affected by non-functional alleles of classical myrosinase and nitrilespecifier protein genes. *Frontiers in Plant Science* 10: 1549.
- Meitzel T, Radchuk R, McAdam EL, Thormählen I, Feil R, Munz E, Hilo A, Geigenberger P, Ross JJ, Lunn JE *et al.* 2021. Trehalose 6-phosphate promotes seed filling by activating auxin biosynthesis. *New Phytologist* 229: 1553–1565
- Mönke G, Seifert M, Keilwagen J, Mohr M, Grosse I, Hähnel U, Junker A, Weisshaar B, Conrad U, Bäumlein H et al. 2012. Toward the identification and regulation of the Arabidopsis thaliana ABI3 regulon. Nucleic Acids Research 40: 8240–8254.
- Monshausen GB, Bibikova TN, Weisenseel MH, Gilroy S. 2009. Ca²⁺ regulates reactive oxygen species production and pH during mechanosensing in *Arabidopsis* roots. *Plant Cell* 21: 2341–2356.
- Munz E, Jakob PM, Borisjuk L. 2016. The potential of nuclear magnetic resonance to track lipids *in planta*. *Biochimie* 130: 97–108.
- Munz E, Rolletschek H, Oeltze-Jafra S, Fuchs J, Guendel A, Neuberger T, Ortleb S, Jakob PM, Borisjuk L. 2017. A functional imaging study of germinating oilseed rape seed. *New Phytologist* 216: 1181–1190.
- Murthy SE, Dubin AE, Patapoutian A. 2017. Piezos thrive under pressure: mechanically activated ion channels in health and disease. *Nature Reviews Molecular Cell Biology* 18: 771–783.
- O'Leary S, Plaxton WC. 2020. Multifaceted functions of post-translational enzyme modifications in the control of plant glycolysis. *Current Opinion in Plant Biology* 55: 28–37.
- O'Neill JP, Colon KT, Jenik PD. 2019. The onset of embryo maturation in *Arabidopsis* is determined by its developmental stage and does not depend on endosperm cellularization. *The Plant Journal* 99: 286–301.
- Park JS, Burckhardt CJ, Lazcano R, Solis LM, Isogai T, Li L, Chen CS, Gao B, Minna JD, Bachoo R et al. 2020. Mechanical regulation of glycolysis via cytoskeleton architecture. Nature 578: 621–626.
- Piccolo S. 2013. Mechanics in the embryo. Nature 504: 223-224.
- Qi H, Xia FN, Xiao S, Li J. 2021. TRAF proteins as key regulators of plant development and stress responses. *Journal of Integrative Plant Biology* 64: 431– 448.
- Radin I, Richardson RA, Coomey JH, Weiner ER, Bascom CS, Li T, Bezanilla M, Haswell ES. 2021. Plant PIEZO homologs modulate vacuole morphology during tip growth. *Science* 373: 586–590.
- Radlanski RJ, Renz H. 2006. Genes, forces, and forms: mechanical aspects of prenatal craniofacial development. *Developmental Dynamics* 235: 1219–1229.
- Rehman HM, Nawaz MA, Shah ZH, Ludwig-Müller J, Chung G, Ahmad MQ, Yang SH, Lee SI. 2018. Comparative genomic and transcriptomic analyses of

- Family-1 UDP glycosyltransferase in three *Brassica* species and *Arabidopsis* indicates stress-responsive regulation. *Science Reports* **30**: 1875.
- Robinson MD, McCarthy DJ, Smyth GK. 2010. EDGER: a bioconductor package for differential expression analysis of digital gene expression data. *Bioinformatics* 26: 139–140.
- Robinson S. 2021. Mechanobiology of cell division in plant growth. New Phytologist 231: 559–564.
- Rolletschek H, Mayer S, Boughton B, Wagner S, Ortleb S, Kiel C, Roessner U, Borisjuk L. 2021a. The metabolic environment of the developing embryo: a multidisciplinary approach on oilseed rapeseed. *Journal of Plant Physiology* 265: 153505
- Rolletschek H, Muszynska A, Borisjuk L. 2021b. The process of seed maturation is influenced by mechanical constraints. *New Phytologist* 229: 19–23.
- Rolletschek H, Schwender J, König C, Chapman KD, Romsdahl T, Lorenz C, Braun HP, Denolf P, Van Audenhove K, Munz E *et al.* 2020. Cellular plasticity in response to suppression of storage proteins in the *Brassica napus* embryo. *Plant Cell* 32: 2383–2401.
- Schneider R, Ehrhardt DW, Meyerowitz EM, Sampathkumar A. 2022.
 Tethering of cellulose synthase to microtubules dampens mechano-induced cytoskeletal organization in *Arabidopsis* pavement cells. *Nature Plants* 8: 1064–1073
- Schwender J, Hebbelmann I, Heinzel N, Hildebrandt T, Naik D, Rogers A, Klapperstück M, Braun HP, Schreiber F, Denolf P et al. 2015. Quantitative multilevel analysis of central metabolism in developing oilseeds of Brassica napus during in vitro culture. Plant Physiology 168: 828–848.
- Sherman BT, Hao M, Qiu J, Jiao X, Baseler MW, Lane HC, Imamichi T, Chang W. 2022. DAVID: a web server for functional enrichment analysis and functional annotation of gene lists (2021 update). *Nucleic Acids Research* 50: W216–W221.
- Tejos R, Rodriguez-Furlán C, Adamowski M, Sauer M, Norambuena L, Friml J. 2018. PATELLINS are regulators of auxin-mediated PIN1 relocation and plant development in *Arabidopsis thaliana*. *Journal of Cell Science* 131: jcs204198.
- Vigeolas H, Waldeck P, Zank T, Geigenberger P. 2007. Increasing seed oil content in oil-seed rape (*Brassica napus* L.) by over-expression of a yeast glycerol-3-phosphate dehydrogenase under the control of a seed-specific promoter. *Plant Biotechnology* 5: 431–441.
- Vogler H, Draeger C, Weber A, Felekis D, Eichenberger C, Routier-Kierzkowska AL, Boisson-Dernier A, Ringli C, Nelson BJ, Smith RS et al.
 2013. The pollen tube: a soft shell with a hard core. The Plant Journal 73: 617–627.
- Willmann MR, Mehalick AJ, Packer RL, Jenik PD. 2011. MicroRNAs regulate the timing of embryo maturation in Arabidopsis. *Plant Physiology* 155: 1871–1884.
- Xu W, Sato H, Bente H, Santos-González J, Köhler C. 2023. Endosperm cellularization failure induces a dehydration-stress response leading to embryo arrest. *Plant Cell* 35: 874–888.
- Yang Z, Liu X, Wang K, Li Z, Jia Q, Zhao C, Zhang M. 2022. ABA-INSENSITIVE 3 with or without FUSCA3 highly up-regulates lipid droplet proteins and activates oil accumulation. *Journal of Experimental Botany* 73: 2077–2092.
- Yatusevich R, Mugford SG, Matthewman C, Gigolashvili T, Frerigmann H, Delaney S, Koprivova A, Flügge UI, Kopriva S. 2010. Genes of primary sulfate assimilation are part of the glucosinolate biosynthetic network in *Arabidopsis thaliana*. The Plant Journal 62: 1–11.

Supporting Information

Additional Supporting Information may be found online in the Supporting Information section at the end of the article.

- **Fig. S1** The experimental setup used to manipulate the space available for the growth of *in vitro* cultured embryos.
- Fig. S2 Dynamics of the growth of seed.

- **Fig. S3** Transcript abundance of selected genes determined using quantitative PCR.
- **Fig. S4** Principal component analysis of the metabolome of *in vivo* grown embryos.
- **Fig. S5** Restriction of the available space transiently accelerates lipid accumulation in the *in vivo* grown embryo.
- Fig. S6 Lipid profiling of embryos grown in vivo.
- **Fig. S7** The effect of space limitation on seed traits at maturity.
- Fig. S8 Effect of space limitation on germination.
- **Methods S1** Collection of files for ready-to-print 3D structures used in the *in vitro* experiments.
- **Methods S2** Proteomics, lipidomics and metabolomics workflows and methods.
- **Table S1** Primers used for quantitative PCR analyses.

- **Table S2** RNA-Seq-derived transcriptome acquired from *in vivo* grown embryos.
- **Table S3** Metabolite abundances in embryos either grown *in vivo* or cultured *in vitro*.
- **Table S4** The lipidome of embryos grown *in vivo* and its statistical test results.
- **Table S5** The proteome of seeds grown *in vivo*.
- **Table S6** RNA-Seq-derived transcriptome acquired from *in vitro* cultured embryos.
- **Video S1** MRI-based virtual model showing seed growth, embryo folding and the developmental dynamics of volume shifts in the endosperm and embryo.

Please note: Wiley is not responsible for the content or functionality of any Supporting Information supplied by the authors. Any queries (other than missing material) should be directed to the *New Phytologist* Central Office.